

Intermittency in two-dimensional turbulence with drag

Yue-Kin Tsang,^{1,2} Edward Ott,^{1,2,3} Thomas M. Antonsen, Jr.,^{1,2,3} and Parvez N. Guzdar²

¹Department of Physics, University of Maryland, College Park, Maryland, 20742 USA

²Institute for Research in Electronics and Applied Physics, University of Maryland, College Park, Maryland, 20742 USA

³Department of Electrical and Computer Engineering, University of Maryland, College Park, Maryland, 20742 USA

(Received 1 June 2004; revised manuscript received 22 March 2005; published 30 June 2005)

We consider the enstrophy cascade in forced two-dimensional turbulence with a linear drag force. In the presence of linear drag, the energy wave-number spectrum drops with a power law faster than in the case without drag, and the vorticity field becomes intermittent, as shown by the anomalous scaling of the vorticity structure functions. Using previous theory, we compare numerical simulation results with predictions for the power law exponent of the energy wave-number spectrum and the scaling exponents of the vorticity structure functions ζ_{2q} . We also study, both by numerical experiment and theoretical analysis, the multifractal structure of the viscous enstrophy dissipation in terms of its Rényi dimension spectrum D_q . We derive a relation between D_q and ζ_{2q} , and discuss its relevance to a version of the refined similarity hypothesis. In addition, we obtain and compare theoretically and numerically derived results for the dependence on separation r of the probability distribution of $\delta_r\omega$, the difference between the vorticity at two points separated by a distance r . Our numerical simulations are done on a 4096×4096 grid.

DOI: 10.1103/PhysRevE.71.066313

PACS number(s): 47.27.Gs, 47.53.+n, 05.45.-a, 83.50.Xa

I. INTRODUCTION

Two-dimensional Navier-Stokes turbulence has attracted much interest because of its relevance to a variety of natural flow phenomena. Examples are plasma in the equatorial ionosphere [1] and the large-scale dynamics of the Earth's atmosphere and oceans [2]. In the laboratory, experiments that are close to two dimensional, such as soap film flow [3,4] and magnetically forced stratified flow [5], have been conducted. In addition, rotating fluid systems [6] are used to study quasi-two-dimensional turbulence and its relevance to large-scale planetary flow. Reference [7] gives a review of some recent experiments in two-dimensional turbulence.

In many of the situations involving two-dimensional turbulence, there are regimes where drag is an important physical effect. In the ionospheric case, there is drag friction of the plasma as it moves relative to the neutral gas background (due to ion-neutral collision). For geophysical flows and rotating fluid experiments, viscosity and the no-slip boundary condition give rise to Ekman friction. In this case the three-dimensional flow is often modeled as two dimensional outside the layer adjoining the no-slip boundary, and the effect of the boundary layer manifests itself as drag in the two-dimensional description. For soap film and magnetically forced flows, friction is exerted on the fluids by surrounding gas and the bottom of the container, respectively. (An experiment is conducted recently to study the effect of bottom friction in magnetically driven flow [8]). In all these cases, the drag force can be modeled as proportional to the two-dimensional fluid velocity \vec{v} , thus the describing Navier-Stokes momentum equation becomes

$$\frac{\partial \vec{v}}{\partial t} + (\vec{v} \cdot \vec{\nabla}) \vec{v} = -\frac{1}{\rho} \vec{\nabla} p + \nu \nabla^2 \vec{v} - \mu \vec{v} + \vec{f}, \quad (1)$$

where ρ is the fluid density, μ is the drag coefficient, ν is the kinematic viscosity, and \vec{f} is an external forcing term. In two

dimensions, the system can be described by the scalar vorticity field ω whose equation of motion is obtained by taking the curl of Eq. (1),

$$\frac{\partial \omega}{\partial t} + \vec{v} \cdot \vec{\nabla} \omega = \nu \nabla^2 \omega - \mu \omega + f_\omega \quad (2)$$

with $\omega = \hat{z} \cdot \vec{\nabla} \times \vec{v}$ and $f_\omega = \hat{z} \cdot \vec{\nabla} \times \vec{f}$, \hat{z} being the unit vector perpendicular to the plane. In our studies, the forcing will be taken to be localized at small wave numbers (k) with a characteristic wave number k_f , and incompressibility, $\vec{\nabla} \cdot \vec{v} = 0$, will be assumed.

According to Kraichnan, for two-dimensional turbulence with no drag and very small viscosity, for $k \gg k_f$, up to the viscous cutoff k_d , enstrophy cascades from small to large k [9]. As a result, the energy wave-number spectrum $E(k)$ has a power law behavior with logarithmic correction [10], $E(k) \sim k^{-3} [\ln(k/k_f)]^{-1/3}$ for $k_f \ll k \ll k_d$. In the presence of a linear drag, the energy spectrum drops with a power law faster than the case with no drag [11–13],

$$E(k) \sim k^{-(3+\xi)} \quad (\xi > 0), \quad (3)$$

and there is no logarithmic correction. A result similar to Eq. (3) has been obtained for the closely related problem of chaotically advected finite lifetime passive scalars [14–16]. (See Sec. II A for a discussion of the relationship between vorticity in two-dimensional turbulence with drag and finite lifetime passive scalars in Lagrangian chaotic flows.)

Furthermore, the vorticity field is intermittent as indicated by (i) anomalous scaling of the *vorticity structure function*, (ii) scale dependence of the *vorticity difference distribution function*, and (iii) multifractal properties of the *enstrophy dissipation field*. Intermittency in the closely related problem of chaotically advected finite lifetime passive scalars was originally studied by Chertkov [14] using a model flow in which the velocity field was spatially linear and δ -correlated

in time (white noise). This model successfully captures the generic intermittent aspect of the problem [17]. With respect to the situation of interest to us in the present paper, it is *a priori* unclear to what extent the δ -correlated model yields results that approximate quantitative results for intermittency measures obtained from experiments (numerical or real). This will be discussed further in Secs. III B and IV.

The structure function of order $2q$, $S_{2q}(\vec{r})$ is defined as the $(2q)$ th moment of the absolute value of the vorticity difference $\delta_{\vec{r}}\omega = \omega(\vec{x} + \vec{r}) - \omega(\vec{x})$. Assuming that the system is homogeneous and isotropic, the structure functions depend on $r = |\vec{r}|$ only. For the case with drag ($\mu > 0$), it is found that, in the enstrophy cascade range ($k_d^{-1} \ll r \ll k_f^{-1}$), $S_{2q}(r)$ scales with r as

$$S_{2q}(r) = \langle |\delta_{\vec{r}}\omega|^{2q} \rangle \sim r^{\xi_{2q}} \quad (4)$$

with $\xi_{2q} > 0$. Furthermore, the vorticity structure functions show anomalous scaling; that is, ξ_{2q} is a nonlinear function of q . The nonlinear dependence of ξ_{2q} on q indicates that the vorticity field is intermittent. In contrast, in the absence of drag ($\mu = 0$), it is predicted that $\omega(\vec{x})$ wiggles rapidly (i.e., on the scale k_d^{-1}) and homogeneously in space. In terms of Eq. (4), this corresponds to $\xi_{2q} = 0$ for $\mu = 0$ [5, 18, 19].

The intermittency of the vorticity field also manifests itself as a change in shape or form of the probability distribution function of the vorticity difference $\delta_{\vec{r}}\omega$ with the separating distance r . It can be shown that if the probability distribution function $\bar{P}_r(X_{\vec{r}})$ of the standardized vorticity difference,

$$X_{\vec{r}} = \frac{\delta_{\vec{r}}\omega}{\sqrt{\langle (\delta_{\vec{r}}\omega)^2 \rangle}}, \quad (5)$$

is independent of r , then ξ_{2q} increases linearly with q : from Eqs. (4) and (5),

$$S_{2q}(r) = \langle |\delta_{\vec{r}}\omega|^{2q} \rangle \int |X_{\vec{r}}|^{2q} \bar{P}_r(X_{\vec{r}}) dX_{\vec{r}}, \quad (6)$$

and, if $\bar{P}_r(X_{\vec{r}})$ is independent of r , for r in the cascade range, then the only r -dependence of $S_{2q}(r)$ comes through the term $\langle |\delta_{\vec{r}}\omega|^{2q} \rangle$, implying $\xi_{2q} = q\xi_2$; that is, ξ_{2q} is linearly proportional to q . Such collapse of $\bar{P}_r(X_{\vec{r}})$ for different values of r has been observed in an experiment [5] where drag is believed to be unimportant. When the effect of drag is not negligible, $\bar{P}_r(X_{\vec{r}})$ changes shape and develops exponential or stretched-exponential tails as r decreases, so that Eq. (6) admits nonlinear dependence of ξ_{2q} on q .

The intermittency of the vorticity field is closely related to the multifractal structure of the viscous enstrophy dissipation field. We define the enstrophy as $\omega^2/2$. From Eq. (2), the time evolution of the enstrophy is then given by

$$\begin{aligned} \frac{\partial}{\partial t} \left(\frac{\omega^2}{2} \right) = & -\vec{\nabla} \cdot \left[\vec{v} \left(\frac{\omega^2}{2} \right) - \nu \vec{\nabla} \left(\frac{\omega^2}{2} \right) \right] - \nu |\vec{\nabla} \omega|^2 - 2\mu \left(\frac{\omega^2}{2} \right) \\ & + \omega f_{\omega}. \end{aligned} \quad (7)$$

We identify the second term on the right hand side of Eq. (7)

as the local rate of viscous enstrophy dissipation η ,

$$\eta = \nu |\vec{\nabla} \omega|^2. \quad (8)$$

The multifractality of the viscous enstrophy dissipation can be quantified by the Rényi dimension spectrum of a measure based on the vorticity gradient. Imagine we divide the region \mathcal{R} occupied by the fluid into a grid of square boxes of size ϵ , we define the measure p_i of the i th box $\mathcal{R}_i(\epsilon)$ as

$$p_i(\epsilon) = \frac{\int_{\mathcal{R}_i(\epsilon)} |\vec{\nabla} \omega|^2 d\vec{x}}{\int_{\mathcal{R}} |\vec{\nabla} \omega|^2 d\vec{x}}. \quad (9)$$

The Rényi dimension spectrum [20] based on this measure is then given by

$$D_q = \frac{1}{q-1} \lim_{\epsilon \rightarrow 0} \lim_{\nu \rightarrow 0} \frac{\ln \sum_i p_i^q}{\ln \epsilon}. \quad (10)$$

The definition Eq. (10) was introduced in the context of natural measures occurring in dynamical systems by Grassberger [21], and Hentschel and Procaccia [22]. In the case with drag, we find that the dimension spectrum for p_i is multifractal; that is, D_q varies with q , in contrast to the case with no drag in which $D_q = 2$, indicating that the measure is uniformly rough.

The subject of this paper is the relation of $\bar{P}_r(X_{\vec{r}})$, the exponents, ξ and ξ_{2q} , and the fractal dimension D_q to the chaotic properties of the turbulent flow [23]. In chaotic flows, the infinitesimal separation between two fluid particle trajectories, $\delta\vec{x}(t)$ typically diverges exponentially. The net rate of exponentiation over a time interval from 0 to t for a trajectory starting at \vec{x}_0 is given by the finite-time Lyapunov exponent h defined as

$$h(t; \vec{x}_0) = \frac{1}{t} \ln \frac{|\delta\vec{x}(t)|}{|\delta\vec{x}(0)|}. \quad (11)$$

At a particular time t , $h(t; \vec{x}_0)$ in general depends on the initial positions \vec{x}_0 and the initial orientation of the perturbation $\delta\vec{x}(0)$. However, for large t , the results for $h(t; \vec{x}_0)$ is insensitive to the orientation of $\delta\vec{x}(0)$ for typical choices of $\delta\vec{x}(0)$, and we neglect the dependence on $\delta\vec{x}(0)$ in what follows. The distribution in the values of h for randomly chosen \vec{x}_0 can be characterized by the conditional probability density function $P(h|t)$.

We perform our simulations on a square domain of size $[-\pi, \pi] \times [-\pi, \pi]$ with periodic boundary conditions in both directions. The viscous term in Eq. (2) is replaced by a hyperviscous damping $-\nu \nabla^8 \omega$ with $\nu = 7.5 \times 10^{-25}$ and $f_{\omega}(x, y) = \cos 2x$ is used for the source function of the vorticity. Our use of a hyperviscosity is similar to what is often done in numerical studies of three-dimensional turbulence and, for a given numerical resolution, has the desirable effect of increasing the scaling range where dissipation can be neglected, while, at the same time it is hoped that this change in the dissipation does not influence the scaling range phys-

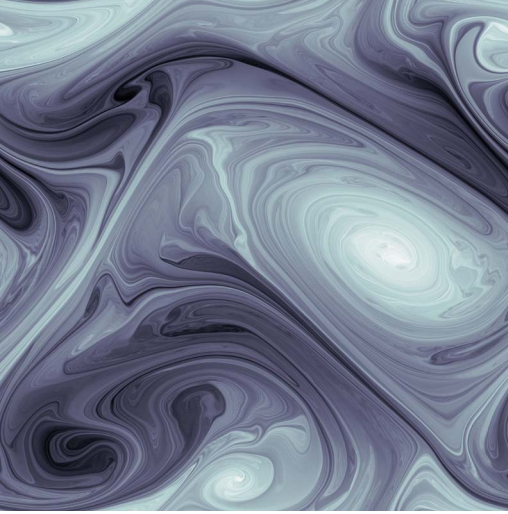


FIG. 1. (Color online) Snapshot of the vorticity field $\omega(x,y)$ at $t=61$ for the case $\mu=0.1$. Light areas are regions of large positive values of the vorticity, and dark areas are regions of negative vorticity of large magnitude.

ics. For wave number $k \leq 6$, we have $\mu=0.1$ and this provides an energy sink at the large scales. For $k > 6$, we will consider the cases of $\mu=0.1$ and $\mu=0.2$. As we shall see in Sec. II A, when drag is present, the large k vorticity components can be considered as being passively advected by the small- k flow components. Applying the same small- k drag (i.e., $\mu=0.1$ for $k \leq 6$) allows us to compare the effects of drag at small scales while keeping similar large scale dynamics of the flows. For all the numerical results presented here, we use a spatial grid of 4096×4096 and a time step of 0.000 25. Starting from random initial conditions for the vorticity field, Eq. (2) is integrated using a time split-step method described in detail in Ref. [24]. The system appears to reach a statistical steady state after about 40 time units. Figure 1 shows a snapshot of the vorticity field for the case of $\mu=0.1$ for all k . At any given moment, there are typically three to five large vortex structures visible in the system. In the steady state, vortices are continuously created and destroyed.

II. ROLE OF THE FINITE-TIME LYAPUNOV EXPONENT

A. Passive nature of the small-scale vorticity

The theory that we will use is based on the approximation that the high k components of the vorticity field are passively advected by the large scale structures of the flow. This can be justified by the following argument given in Ref. [12]. The Lyapunov exponent h of the flow is the mean rate of exponentiation of differential displacement $\delta\vec{x}$ following the flow, where $d(\delta\vec{x})/dt = \delta\vec{x} \cdot \vec{\nabla}\vec{v}$. Thus one can crudely estimate the Lyapunov exponent as

$$h \sim \langle \|\vec{\nabla}\vec{v}\|^2 \rangle^{1/2} \sim \sqrt{\int_{k_f}^{\infty} k^2 E(k) dk}, \quad (12)$$

where $\|\vec{\nabla}\vec{v}\|^2 = (\partial v_x / \partial x)^2 + (\partial v_y / \partial y)^2 + (\partial v_x / \partial y)^2 + (\partial v_y / \partial x)^2$. Assuming the limit of infinite Reynolds number and power

law behavior of $E(k)$ valid as $k \rightarrow \infty$, the integral in Eq. (12) diverges at the upper limit unless ξ in Eq. (3) is positive. That is, the velocity field \vec{v} is not differentiable (h and $\vec{\nabla}\vec{v}$ are undefined) unless $\xi > 0$ (alternatively, if $\xi < 0$ and viscosity imposes a cutoff to power law behavior of $E(k)$ at $k \sim k_d$, then, although $\|\vec{\nabla}\vec{v}\|^2$ is now finite, the integral in Eq. (12) is dominated by velocity components at the shortest wavelength). From Eq. (12), for $\xi > 0$, we have $h \sim k_f^{-\xi/2}$. This means that h , which characterizes small scale stretching, is determined by the largest scale flow components. Since $\xi > 0$ in the case where drag is present, $\vec{\nabla}\vec{v}$ is predominantly determined by the largest spatial scales. Thus the Lyapunov exponents provide information on the evolution of the distance between fluid elements whose separation is *finite* but small compared to k_f^{-1} . This will allow us to approximate the evolution of vorticity field components with wave numbers in the range $k_f \ll k < k_d$ using Lyapunov exponents that result primarily from the large spatial scales $k \sim k_f$. That is, the vorticity field at wave number $k_f \ll k < k_d$ evolves via approximately passive advection by the large scale flow. (Note that for $\xi < 0$ such an approach would not be applicable since the Lyapunov numbers would provide an estimate of separation evolution only for distances less than k_d^{-1} which is outside the dissipationless power law range.)

Note that the case without drag corresponds to $\xi=0$, which is marginal in the sense that it is on the borderline of the condition for differentiability of the velocity field. In other situations of marginality (e.g., in critical phenomena), it is often found that there are logarithmic corrections to power-law scaling, and this may be thought of as the origin of Kraichnan's logarithmic correction to the k^{-3} enstrophy cascade scaling of $E(k)$.

B. Distribution of finite-time Lyapunov exponent

As mentioned earlier, the exponential divergence of nearby trajectories in a chaotic flow over a time interval 0 to t can be quantified by a finite-time Lyapunov exponent $h(t; \vec{x}_0)$ defined in Eq. (11). In the limit $t \rightarrow \infty$, $h(t; \vec{x}_0)$ will approach the usual infinite-time Lyapunov exponent \bar{h} for almost all initial conditions \vec{x}_0 and almost all initial orientations of $\delta\vec{x}$. At finite time, the dependence of h on \vec{x}_0 results in a distribution in the values of h which can be characterized by the probability density function $P(h|t)$. That is, if \vec{x}_0 is chosen randomly with uniform density in the region of the fluid flow, and if the initial orientation of $\delta\vec{x}$ is arbitrarily chosen, then we can define a probability distribution $P(h|t)$ such that $P(h|t)dh$ is the probability that $h(t; \vec{x}_0)$ lies between h and $h+dh$. As t increases, $P(h|t)$ will become more and more sharply peaked at \bar{h} and approach a delta function at \bar{h} as $t \rightarrow \infty$. We use the procedures described in Ref. [24] to numerically obtain histogram approximations to $P(h|t)$ (not shown).

Based on the argument that $h(t; \vec{x}_0)$ can be considered as an average over many independent random realizations, $P(h|t)$ is approximated by the following asymptotic form ([25] and references therein):

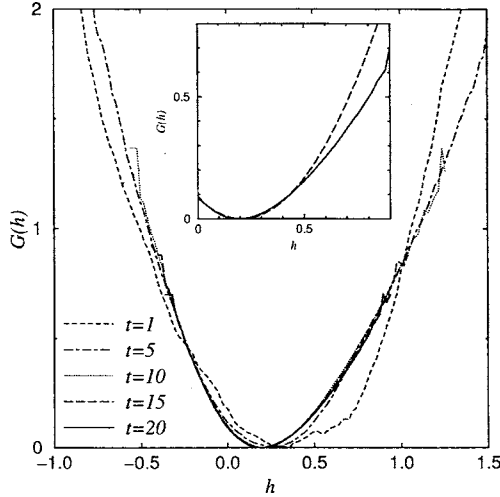


FIG. 2. $G(h)$ [see Eq. (13)] for different time t for the case $\mu(k>6)=0.2$. The inset shows $G(h)$ obtained at $t=20$ (solid line) and the quadratic approximation to $G(h)$ obtained by the method described at the end of Sec. III B (dashed line).

$$P(h|t) \sim \sqrt{\frac{tG''(h)}{2\pi}} e^{-tG(h)} \quad (13)$$

for large t . Equation (13) has been shown to be true for the generalized baker's map [26] and numerically verified for cases where there are no Kolmogorov-Arnold-Moser (KAM) surfaces, for example, see Ref. [27]. The function $G(h)$ is concave upward, $G''(h) \geq 0$. It has the minimum value zero, occurring at $h=\bar{h}$, $G'(\bar{h})=G(\bar{h})=0$. We note that $G(h)$ is completely specified by the flow $\vec{v}(\vec{x}, t)$ and hence is dependent on the value of μ .

The function $G(h)$ can be approximated at large t from $P(h|t)$ using the following relation:

$$G(h) \approx K - \frac{1}{t} \ln P(h|t), \quad (14)$$

where K is determined by the condition that the minimum of $G(h)$ equals zero. Figure 2 shows the $G(h)$ obtained from our flow with $\mu(k>6)=0.2$. The large number (4096^2) of fluid trajectories used in the generation of each $P(h|t)$ allows us to obtain $G(h)$ for a large range of h . As can be seen in Fig. 2, for large enough t , the graphs of $G(h)$ for different t more or less collapse onto each other, showing that Eq. (13) is a good approximation to $P(h|t)$ for the flows we considered. $G(h)$ shows similar behavior in the case $\mu=0.1$.

III. EXPONENTS ξ AND ζ_{2q}

A. Review of theory

We consider the scaling of the vorticity structure functions in the limit $\nu \rightarrow 0^+$. The result has previously been given in Ref. [28], which treats finite-lifetime passive scalars [14–16] rather than vorticity in two-dimensional turbulence with drag, and in Ref. [29] for two-dimensional turbulence with drag.

The result from Ref. [28] for the structure function exponent ζ_{2q} is

$$\zeta_{2q} = \min_h \{2q, H_q(h)\}, \quad (15)$$

where

$$H_q(h) = \frac{G(h) + 2q\mu}{h}. \quad (16)$$

Equations (15) and (16) yield the previous passive scalar result of Ref. [14] if $G(h)$ is assumed parabolic, $G(h) = (\text{const}) \times (h - \bar{h})^2$, which is a consequence of the temporally white noise velocity field model of Ref. [14].

We now consider the energy density $e(\vec{k})$ which is given by

$$e(\vec{k}) = \frac{1}{(2\pi)^2} \frac{|\tilde{v}_x(\vec{k})|^2 + |\tilde{v}_y(\vec{k})|^2}{2L^2}, \quad (17)$$

where $\tilde{v}_x(\vec{k})$ and $\tilde{v}_y(\vec{k})$ are Fourier transforms of the x and y components of the velocity field $\vec{v}(x, y)$. The wave-number energy spectrum $E(k)$ is then defined as

$$E(k) = \int d\vec{k}' \delta(|\vec{k}'| - k) e(\vec{k}'). \quad (18)$$

A previous theory [11,12] relates the energy wave-number spectrum exponent ξ defined in Eq. (3) to $G(h)$. The result is

$$\xi = \min_h \{H_1(h)\}, \quad (19)$$

where H_1 is given by Eq. (16) with $q=1$. Thus ξ and ζ_{2q} are related to the properties of the flow, namely the drag coefficient μ and the distribution of the finite-time Lyapunov exponent h .

B. Comparison of theory and numerical results

To apply the theory Eqs. (15) and (19) to numerically determine the exponents ζ_{2q} and ξ of our turbulent flow governed by Eq. (2), we first let

$$\bar{\zeta}_{2q} = \min_h \{H_q(h)\}. \quad (20)$$

Using Eq. (16), we rewrite Eq. (20) as

$$\min_h \left\{ \frac{G(h) + 2q\mu}{h} - \bar{\zeta}_{2q} \right\} = 0. \quad (21)$$

Since the function minimized in Eq. (21) has minimum value zero, we can multiply it by any positive function of h , and the minimum will still be zero. Thus for $h>0$ we can multiply the minimized function by h to obtain

$$\min_h \{G(h) - h\bar{\zeta}_{2q}\} = -2q\mu. \quad (22)$$

Using Eqs. (13) and (22), we see that steepest descent evaluation of the following integral for large t yields

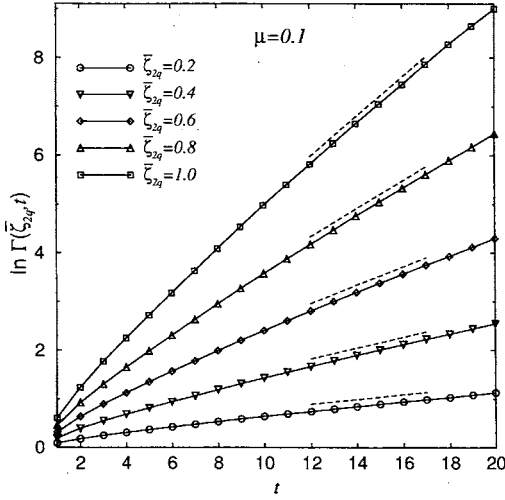


FIG. 3. Log-linear plot of the partition function $\Gamma(\bar{\xi}_{2q}, t)$ for $\mu=0.1$. The dotted lines are linear fits.

$$\int P(h|t) e^{h\bar{\xi}_{2q}t} dh \sim e^{2q\mu t}. \quad (23)$$

Thus we define the partition function [30]

$$\Gamma(z, t) = \int e^{zh(t; \vec{x}_0)t} d\vec{x}_0, \quad (24)$$

in terms of which Eq. (23) becomes

$$\Gamma(\bar{\xi}_{2q}, t) \sim e^{2q\mu t}. \quad (25)$$

We numerically compute the partition function Eq. (24) using the approximation

$$\Gamma(z, t) = \frac{1}{M} \sum_{i=1}^M e^{zh(t; \vec{x}_{0i})t} \quad (26)$$

employing many ($M=4096^2$) spatially uniformly distributed initial conditions \vec{x}_{0i} ($i=1, 2, \dots, M$).

For different values of $\bar{\xi}_{2q}$, we then plot $\ln \Gamma(\bar{\xi}_{2q}, t)$ vs t . Figure 3 shows samples of $\ln \Gamma(\bar{\xi}_{2q}, t)$ for the case $\mu=0.1$. As expected, for large t , $\ln \Gamma(\bar{\xi}_{2q}, t)$ is linear in t and the slope, which can be estimated using a linear fit, gives the corresponding value of q for each $\bar{\xi}_{2q}$. Figure 4 plots $\bar{\xi}_{2q}$ vs q obtained in this way for $\mu=0.1$ and $\mu(k>6)=0.2$ (open circles and squares) together with the corresponding sixth degree polynomial fits (solid lines). By Eqs. (15) and (19), the exponents ξ and ζ_{2q} can then be determined from Fig. 4 by $\xi = \bar{\xi}_2$ and $\zeta_{2q} = \min\{2q, \bar{\xi}_{2q}\}$.

It is also possible to compute ξ and ζ_{2q} directly from Eqs. (15) and (19) using a fourth degree polynomial fit of the numerically obtained $G(h)$. We find that the two methods give similar results, but that the method of Eq. (26) is easier to compute.

We also test the applicability of the result of Ref. [14], which employs a model in which the velocity field is δ -correlated in time. This model may be shown to corre-

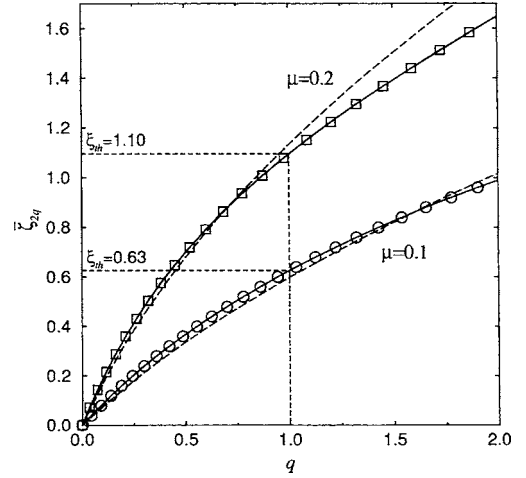


FIG. 4. $\bar{\xi}_{2q}$ as a function of q from the method of Fig. 3 for $\mu=0.1$ (circles) and $\mu(k>6)=0.2$ (squares). The solid lines are sixth degree polynomial fits to circles and squares. Results using Eq. (5) of Ref. [14] are shown as dashed lines.

spond to Eqs. (15) and (16) with $G(h)$ parabolic, $G(h) = a(h - \bar{h})^2$ where \bar{h} is the infinite time Lyapunov exponent. With this form of $G(h)$, an explicit analytic expression for the structure function exponents can be obtained in terms of the constant a and \bar{h} ; see Eq. (5) of Ref. [14]. In order to apply this result to a specific flow, we need to formulate a procedure for obtaining a reasonable value of a from the flow (\bar{h} is well defined and numerically accessible by standard technique). For this purpose, we note that, within the δ -correlated approximation, the total exponentiation $h(t; \vec{x}_0)t$ experienced by an infinitesimal vector originating at position \vec{x}_0 undergoes a random walk with diffusion constant $D = a/4$. Thus we obtain a as one-half of the long time slope of a plot of $\langle (h - \bar{h})^2 \rangle t^2$ vs t . The inset to Fig. 2 shows as a solid curve $G(h)$ obtained using Eq. (14) (as previously described) along with the parabolic model (dashed curve) with a determined by the above procedure. There appears to be a substantial difference in the important range $h > \bar{h}$ where the saddle points are located. Somewhat surprisingly, however, this does not lead to much difference in the numerical values of the structure function exponents. This is shown in Fig. 4 where the results using Eq. (5) of Ref. [14] are plotted as dashed curves. In fact, the difference is within the error of our numerical experiments that directly determine the values of $\bar{\xi}_{2q}$. Thus for this case the parabolic approximation provides an adequate fit to the data, although this could not be definitely predicted *a priori*.

1. Energy wave-number spectrum

As illustrated in Fig. 4, theoretical predictions for ξ , denoted as ξ_{th} , are obtained using the method described above. The results are given in Table I. To verify the theoretical results, we compute the energy spectrum directly from the numerical solution of Eq. (2) on a 4096×4096 grid using Eq. (18), which can be written in terms of the vorticity as

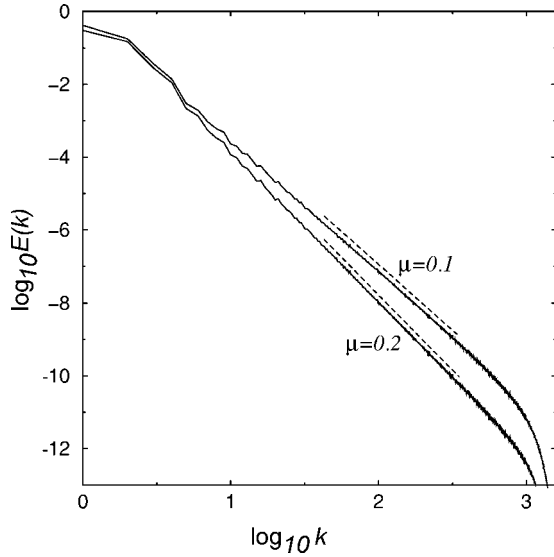


FIG. 5. Energy wave-number spectra. The dotted lines are the corresponding linear fit in the scaling range.

$$E(k, t) = \int \frac{d\vec{k}'}{(2\pi L)^2} \delta(|\vec{k}'| - k) \frac{|\tilde{\omega}(\vec{k}', t)|^2}{2|\vec{k}'|^2}, \quad (27)$$

where $\tilde{\omega}(\vec{k}', t)$ is the Fourier transform of $\omega(\vec{x}, t)$. The time averaged energy spectrum $E(k)$ is obtained by averaging $E(k, t)$ at every 0.1 time unit from $t=41$ to $t=75$. Figure 5 shows a log-log plot of $E(k)$ versus k for the two different values of $\mu(k > 6)$ we considered. In both cases, a clear scaling range of more than a decade can be observed. We measure the scaling exponents by linearly fitting $E(k)$ in the scaling range. The results, denoted ξ_{DNS} , are shown in Table I. Good agreement is found between the numerical and the theoretical results. These results are consistent with those of previous work in Refs. [12,29] which use grids of 1024×1024 and 2048×2048 , respectively.

2. Vorticity structure functions

Numerical tests of theoretical predictions of structure function exponents of finite-lifetime passive scalar fields ad-

TABLE I. Comparison of the values of ξ obtained from numerical simulations to the theoretical results.

$\mu(k > 6)$	$\xi_{th.} (= \xi_{2,th.})$	ξ_{DNS}	$\xi_{2,DNS}$
0.1	0.63	0.61	0.66
0.2	1.10	1.12	1.16

vected by simple chaotic flows have been performed in Refs. [28,29]. To test the analogous theoretical predictions, Eqs. (15) and (16), in the case of two-dimensional turbulence with drag, we define the averaged structure functions of order $2q$ as

$$S_{2q}(r) = \int \frac{d\vec{r}'}{2\pi r} \delta(r - |\vec{r}'|) \langle |\delta_{\vec{r}'} \omega|^{2q} \rangle. \quad (28)$$

The angle brackets denote average over the entire region occupied by the fluid. The angular dependence of $\langle |\delta_{\vec{r}'} \omega|^{2q} \rangle$ is averaged out in Eq. (28) by the integration over \vec{r}' . Using Eq. (28) with $\omega(\vec{x}, t)$ obtained from the numerical integration of Eq. (2), we compute $S_{2q}(r)$ from $t=41$ to $t=75$ at every 1 time unit and take the average of the results obtained.

Following the scheme described above, we calculate the time-averaged structure functions for q ranging from 0.0 to 2.0. Figure 6(a) shows samples of the results for the case $\mu=0.1$. The distance r is measured in the unit of grid size. For all values of q we have studied, the structure functions show a clear scaling range that is long enough to allow an estimate of the scaling exponents, ζ_{2q} . The scaling range of the structure functions in real space roughly corresponds to that of the energy spectrum in k space. The values of ζ_{2q} are obtained by measuring the slope of the structure functions in the scaling range using a linear fit. Results for ζ_{2q}/ζ_2 are shown as circles in Figs. 6(b) and 6(c). The measured values of ζ_2 , denoted as $\zeta_{2,DNS}$, are given in Table I. We then obtain theoretical predictions to ζ_{2q} from the polynomial fit of $\bar{\zeta}_{2q}$ shown in Fig. 4, following procedures described at the beginning of this section. The results are shown as crosses in

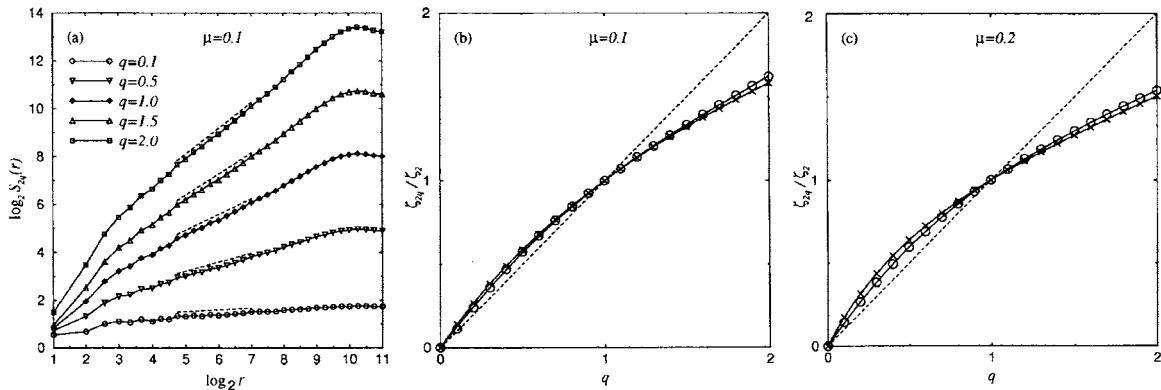


FIG. 6. For the case of $\mu=0.1$, (a) structure functions of vorticity difference, for various orders q between 0.1 and 2.0; the dotted lines are linear fits in the scaling range. (b) Plot of ζ_{2q}/ζ_2 obtained from numerical simulations (circle) and from Eq. (15) (crosses), for different values of q ; the solid lines are polynomial fits to the circles and the crosses [cf. Eq. (43)]. (c) Plot of ζ_{2q}/ζ_2 for the case of $\mu(k > 6)=0.2$ obtained from numerical simulations (circles) and from Eq. (15) (crosses), for different values of q ; the solid lines are polynomial fits to the circles and the crosses.

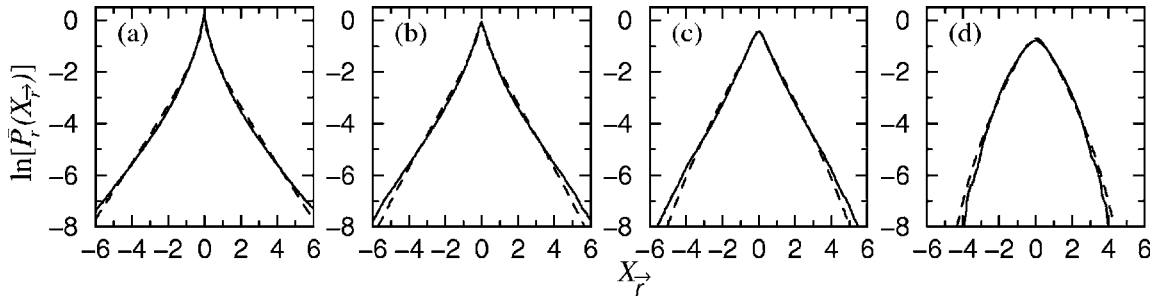


FIG. 7. For $\mu=0.1$, the probability distribution function $\bar{P}_r(X_{\vec{r}})$ of the standardized vorticity difference $X_{\vec{r}}$ obtained from direct numerical simulation (solid lines) and from Eq. (29) (dashed lines). The separating distance \vec{r} is in the \hat{x} direction and measured in the unit of grid size: (a) $r=4$; (b) $r=16$; (c) $r=64$; (d) $r=512$.

Figs. 6(b) and 6(c) for the two cases of μ we studied. The predicted values of ζ_2 , denoted as $\zeta_{2,th}$, are given in Table I. The numerical and theoretical results agree reasonably well for all q 's. In reference to Eq. (15) we note that, for all the cases we numerically tested, we found that $\zeta_{2q} = \bar{\zeta}_{2q} < 2q$ for all q . This is consistent with the general result that for $\mu < \bar{h}$, $\bar{\zeta}_{2q} < H_q(\bar{h}) < 2q$. We note, however, that this need not hold in general, particularly for large μ .

IV. PROBABILITY DISTRIBUTION OF VORTICITY DIFFERENCE

Theory

A partial differential equation for the probability distribution $P_r(\delta_{\vec{r}}\omega)$ of the vorticity difference $\delta_{\vec{r}}\omega$ has been derived in Ref. [14] for the case of a δ -correlated velocity field. As previously discussed, this case corresponds to a parabolic $G(h)$. In the more general case of a nonparabolic $G(h)$, it can be shown [23] that

$$P_r(\delta_{\vec{r}}\omega) = \int_0^\infty \frac{1}{y(\tau)} P_L \left[\frac{\delta_{\vec{r}}\omega}{y(\tau)} \right] \left\{ \frac{d}{d\tau} \int_{\frac{\lambda}{\tau}}^\infty dh P(h|\tau) \right\} d\tau, \quad (29)$$

where $y(\tau) = (e^{-\lambda} + e^{-\mu\tau})/2$ and P_L denotes the probability distribution P_r at $r=L$. Thus Eq. (29) gives P_r for $r < L$ in terms of its ‘‘boundary value’’ at $r=L$. Reference [14] gives an integral expression for $P_r(\delta_{\vec{r}}\omega)$ for the δ -correlated model and the illustrative case where P_L is Gaussian.

In order to obtain reasonable agreement between the theory Eq. (29) and our numerical experiments, it is important to account for the non-Gaussian behavior of the probability distribution function of the vorticity difference at large separation $|\vec{r}|$. In what follows, this will be done by using the numerically obtained probability distribution function at large $|\vec{r}|$ as an input to Eq. (29) to determine the probability distribution function at small $|\vec{r}|$. On the other hand, as mentioned in Sec. III, the parabolic approximation for $G(h)$ results in an adequate fit of the numerical structure function exponent data to the theoretical prediction. We thus use $G(h) \approx a(h-\bar{h})^2$ with a determined as in Sec. III.

We first compute the probability distribution function $\bar{P}_r(X_{\vec{r}})$ of the standardized vorticity difference $X_{\vec{r}}$, Eq. (5),

directly from the numerical solution of Eq. (2). The vorticity field $\omega(\vec{x}, t)$ from $t=41$ to $t=75$ at every 1 time unit is used in this computation. The separating distance \vec{r} is taken to be in the \hat{x} direction and is measured in the unit of grid size. For $\mu=0.1$, the results for four different values of r are shown as solid lines in Fig. 7. It is clear that the shape of $\bar{P}_r(X_{\vec{r}})$ changes as r varies in the range $4 \leq r \leq 512$, indicating the system is intermittent. $\bar{P}_r(X_{\vec{r}})$ develops exponential tails (e.g., $r=64$) and then stretched-exponential tails (e.g., $r=4$) as r decreases. Numerical results similar to those in Fig. 7 have also been obtained in Ref. [29], but theory for $\bar{P}_r(X_{\vec{r}})$ was not presented in Ref. [29].

To apply the theoretical result Eq. (29), we take P_L in Eq. (29) to be of the form $\exp(W)$ where W is an even sixth degree polynomial fitted to the numerically computed $\ln[P_r(\delta_{\vec{r}}\omega)]$ for $\vec{r}=1024\hat{x}$ and $\mu=0.1$. We then compute $P_r(\delta_{\vec{r}}\omega)$, and thus $\bar{P}_r(X_{\vec{r}})$, for different values of r using Eq. (29). The results are plotted as dashed lines in Fig. 7. The theoretical predictions agree well with the numerical results. We also find good agreements between theory and numerical simulations when \vec{r} is taken to be in the \hat{y} direction. Similar results were also obtained for the case $\mu(k>6)=0.2$.

V. MULTIFRACTAL FORMULATION

A. Theory

The local viscous energy dissipation rate per unit mass ε and its global average value $\langle \varepsilon \rangle$ play important roles in the phenomenology of three-dimensional turbulence [31]. It is now well known that ε shows intermittent spatial fluctuations which can be described by the multifractal formulation [32]. Using the measure $p'(r) = \mathcal{E}_r / \mathcal{E}$, where \mathcal{E}_r is the total dissipation in a volume of linear dimension r and \mathcal{E} is the total dissipation in the whole domain, the Rényi dimension spectrum D_q and the singularity spectrum $f(\alpha)$ have been measured experimentally [33,34].

Intermittency in three-dimensional turbulence also manifests itself as anomalous scaling in the velocity structure functions $S'_{3q}(r)$ defined as

$$S'_{3q}(r) = \langle (\delta_{\vec{r}}v)^{3q} \rangle \sim r^{\zeta'_{3q}}, \quad (30)$$

where v is the component of the velocity vector in the direction of \vec{r} and $\delta_{\vec{r}}v = v(\vec{x}+\vec{r}) - v(\vec{x})$. From Kolmogorov's hy-

potheses in his 1941 paper [35], which ignore the intermittency of ε , one arrives at the result $\zeta'_{3q}=q$. Experiments show that ζ'_{3q} is a nonlinear function of q . This anomalous scaling of $S'_{3q}(r)$ is believed to be related to the intermittency of ε . Kolmogorov's "refined similarity hypothesis" in his 1962 paper [36] gives the connection between intermittency in velocity difference and intermittency in ε . The refined similarity hypothesis states that at very high Reynolds numbers, there is an inertial range of r in which the conditional moments of $\delta_r v$ scales as follows:

$$\langle (\delta_r v)^q | \varepsilon_r \rangle \sim (r \varepsilon_r)^{q/3}, \quad (31)$$

where ε_r is the average of ε over a volume of linear dimension r . Equation (31) implies $\langle (\delta_r v)^q \rangle \sim \langle (r \varepsilon_r)^{q/3} \rangle$ which gives the following relation between the D_q based on $p'(r)$ and ζ'_{3q} :

$$D_q = 3 + \frac{\zeta'_{3q} - q\zeta'_3}{q-1}. \quad (32)$$

Kolmogorov's fourth-fifths law gives $\zeta'_3=1$ exactly [32]. Equation (32) can also be derived [34] from the relation

$$\varepsilon_r \sim \frac{(\delta_r v)^3}{r}. \quad (33)$$

We note that Eq. (31) follows from Eq. (33). As shown below, there is a relation analogous to Eq. (32) for the enstrophy cascade of two-dimensional turbulence with drag.

For the enstrophy cascade regime in two-dimensional turbulence, a central quantity to the phenomenology [9] in this regime is the viscous enstrophy dissipation η given by Eq. (8), and the relevant measure is $p_i(\epsilon)$ defined in Eq. (9). We have already seen in Sec. III that in the presence of drag, the vorticity structure functions scale anomalously with scaling exponents ζ_{2q} given by Eq. (15). We now derive a relation between ζ_{2q} and the D_q based on $p_i(\epsilon)$.

Consider the following quantity:

$$I_1(q, \epsilon) = \sum_i p_i^q(\epsilon) \quad (34)$$

which by the definition of D_q , Eq. (10), scales like

$$I_1(q, \epsilon) \sim \epsilon^{(q-1)D_q} \quad (35)$$

for some range of ϵ . Assume there exists a scaling range extending from the system scale $L \sim k_f^{-1}$ down to the dissipative scale $r_d \sim k_d^{-1}$ such that both the scaling relations Eqs. (4) and (35) hold. At the dissipative scale, due to the action of viscosity, the vorticity field ω becomes smooth, thus we have the following relations:

$$\int_{\mathcal{R}(r_d)} |\vec{\nabla} \omega|^2 d\vec{x} \sim r_d^2 |\vec{\nabla} \omega(\vec{x})|^2, \quad \vec{x} \in \mathcal{R}(r_d), \quad (36)$$

$$|\vec{\nabla} \omega| \sim \frac{|\delta_r \omega|}{r_d}, \quad |\vec{r}| = r_d. \quad (37)$$

Then by putting $\epsilon=r_d$ in Eq. (9) and let $|\vec{r}|=r_d$ and $\vec{x}_i \in \mathcal{R}_i(r_d)$, we get

$$p_i(r_d) \sim \frac{|\delta_r \omega(\vec{x}_i)|^2}{(r_d)^{-2} \int_{\mathcal{R}} |\delta_r \omega|^2 d\vec{x}}. \quad (38)$$

Substituting Eq. (38) in Eq. (34), we obtain the scaling of $I_1(q, \epsilon)$,

$$\begin{aligned} I_1(q, r_d) &\sim \frac{\sum_i |\delta_r \omega(\vec{x}_i)|^{2q}}{\left(\frac{1}{(r_d)^{2q}} \left(\int_{\mathcal{R}} |\delta_r \omega|^2 d\vec{x} \right)^q \right)} \\ &\sim \left(\frac{L}{r_d} \right)^{2q} \langle |\delta_r \omega|^{2q} \rangle \\ &\sim \left(\frac{L}{r_d} \right)^{2q} \langle |\delta_r \omega|^2 \rangle^q \\ &\sim (r_d)^{2q-2+\zeta_{2q}-q\zeta_2}. \end{aligned} \quad (39)$$

Comparing Eq. (35) to Eq. (39), we get the principal result of this section,

$$D_q = 2 + \frac{\zeta_{2q} - q\zeta_2}{q-1}, \quad (40)$$

which can be regarded as analogous to Eq. (32).

We mention that Eq. (32) can be derived in an analogous manner using Eq. (33). From Eq. (40), in two-dimensional turbulence, the measure p_i is multifractal when the vorticity structure functions exhibit anomalous scaling. Hence, in the presence of drag, we expect the measure based on the squared vorticity gradient $|\vec{\nabla} \omega|^2$ to show multifractal structures.

B. Comparison of theory and numerical results

The multifractal structure of $|\vec{\nabla} \omega|^2$ is most readily visualized in snapshots of $|\vec{\nabla} \omega|^2$ from our simulations. Since $|\vec{\nabla} \omega|^2$ grows at widely varying exponential rates, only a few points would be visible if $|\vec{\nabla} \omega|^2$ was plotted directly using a linear scale. Therefore we plot the following quantity instead [27]:

$$\mathcal{M}(\vec{x}) = \frac{\sum_{\vec{x}_i \in \Lambda_{\vec{x}}} |\vec{\nabla} \omega(\vec{x}_i)|^2}{\sum_i |\vec{\nabla} \omega(\vec{x}_i)|^2}, \quad (41)$$

where the set $\Lambda_{\vec{x}}$ contains those lattice points \vec{x}_i for which $|\vec{\nabla} \omega(\vec{x}_i)|^2 \leq |\vec{\nabla} \omega(\vec{x})|^2$, and we sum over all lattice points in the denominator. By definition, $0 \leq \mathcal{M}(\vec{x}) \leq 1$. Figure 8 shows the result for $\mu=0.1$. Filament structures can clearly be seen, showing that the measure p_i concentrates in a very small area.

To quantify the multifractal nature of p_i , we now calculate its Rényi dimension spectrum D_q . We employ the box-counting method to estimate D_q . Using box size ϵ/L ranging from 2^{-12} to 2^{-1} , we compute the instantaneous $I_1(q, \epsilon)$ from $t=41$ to $t=75$ at every 1 time unit using the numerical solution of Eq. (2). For $q \neq 1$, we then make log-log plot of the time-average of $[I_1/(q-1)]$ vs ϵ/L . These are shown in Fig.

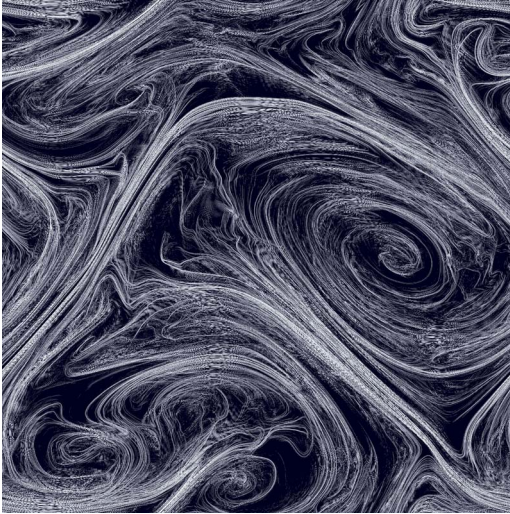


FIG. 8. (Color online) Snapshots of the scaled squared vorticity gradient $|\vec{\nabla}\omega|^2$ at $t=61$ for the case $\mu=0.1$. Light areas are regions of large values, and dark areas are regions of small values.

9(a). For $q=1$, we take the limit $q \rightarrow 1$ in Eq. (35) to obtain $I_2(\epsilon) \sim \epsilon^{D_1}$, where

$$I_2(\epsilon) = \sum_i p_i(\epsilon) \log_2[p_i(\epsilon)], \quad (42)$$

and for $q=1$ in Fig. 9(a), the time average of $I_2(\epsilon)$ is plotted against $\log_2(\epsilon/L)$. According to Eq. (35), these plots will show a linear region with slope equals D_q . All curves in Fig. 9(a) show slightly undulating behavior which introduces uncertainties in the determination of D_q . The estimated D_q at different values of q are shown as circles with error bars in Figs. 9(b) and 10. The error bars correspond to the variability of the D_q observed at different moments in time. The dotted lines in the figures are fourth degree polynomials fitted to the circles. We also compute D_q using Eq. (40). To this end, we fit the curves of ζ_{2q}/ζ_2 vs q in Figs. 6(b) and 6(c) with the following polynomial, where $d=3$ for the circles and $d=5$ for the crosses:

$$\frac{\zeta_{2q}}{\zeta_2} = q \left[1 + \sum_{n=1}^d a_n (q-1)^n \right]. \quad (43)$$

By Eq. (40), D_q is then given by

$$D_q = 2 + \zeta_2 \sum_{n=1}^d a_n q (q-1)^{n-1}. \quad (44)$$

In Figs. 9(b) and 10, we plot Eq. (44) using ζ_{2q} obtained from numerical simulations, as well as ζ_{2q} calculated from our theory. The results are shown as solid lines labeled with squares and diamonds, respectively. Despite the fact that there are discrepancies between the D_q obtained by the various methods, they all show the same trend and clearly indicates that p_i is multifractal (i.e., D_q varies with q).

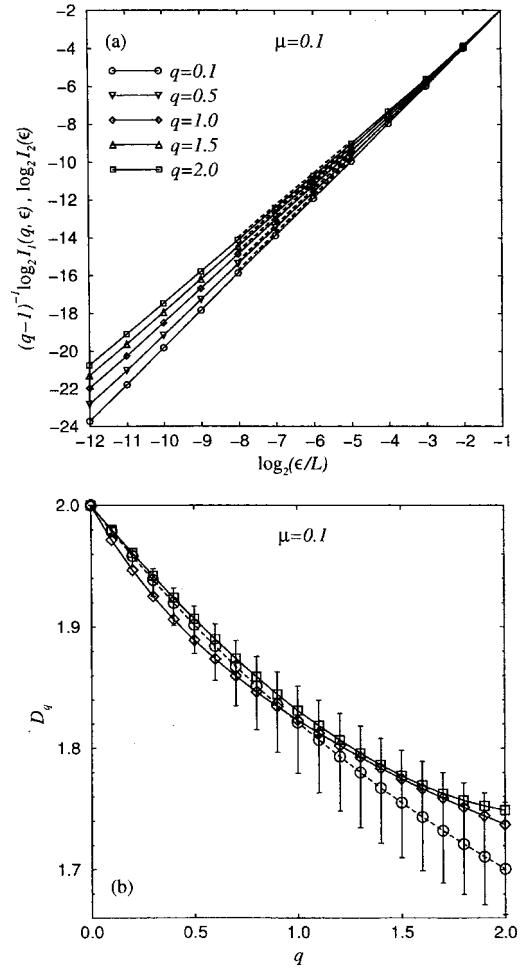


FIG. 9. For the case of $\mu=0.1$, (a) $I_1(q, \epsilon)$ for q between 0.1 and 2.0 [$I_2(\epsilon)$ is plotted for $q=1.0$]. The dotted lines are linear fits in the scaling region [similar results are obtained for $\mu(k>6)=0.2$]. (b) D_q computed using numerical solution of Eq. (2) (circle with error bar) and its fourth degree polynomial fit (dotted line). D_q predicted by the theory Eq. (40) when ζ_{2q} obtained from numerical simulations are used (square) and when ζ_{2q} calculated from Eq. (15) are used (diamond).

C. Discussion

Kolmogorov introduced the refined similarity hypothesis (RSH) Eq. (31) to take into account the spatial fluctuations of ϵ in three-dimensional turbulence. The relation Eq. (32) is a direct consequence of the RSH. In two-dimensional turbulence, the relevant quantity is the local rate of viscous enstrophy dissipation η . We have already seen that the measure p_i is multifractal in the presence of drag, indicating the intermittent nature of η . Following Kolmogorov's ideas, we consider the average of η over an area $\mathcal{R}(r)$ of linear dimension r :

$$\eta_r = \frac{\nu}{r^2} \int_{\mathcal{R}(r)} |\vec{\nabla}\omega|^2 d\vec{x}. \quad (45)$$

Analogous to the Kolmogorov's RSH, we propose that at high Reynolds number, there is an inertial range of r in which

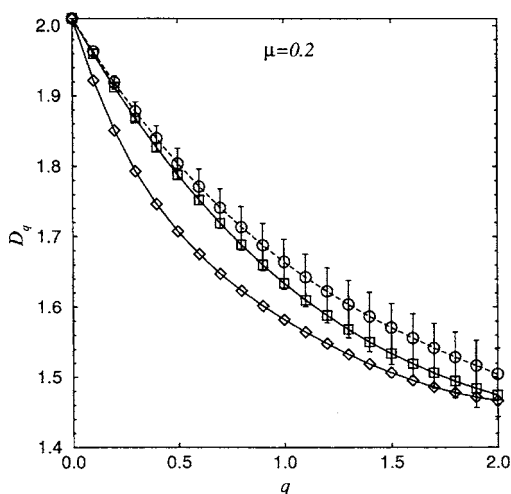


FIG. 10. D_q for the case of $\mu(k > 6) = 0.2$, computed using numerical solution of Eq. (2) (circle with error bar) and its fourth degree polynomial fit (dotted line). D_q predicted by the theory Eq. (40) when ζ_{2q} obtained from numerical simulations are used (square) and when ζ_{2q} calculated from Eq. (15) are used (diamond).

$$\langle |\delta_{\vec{r}} \omega|^{2q} | \eta_r \rangle = C_{2q} (r^{\zeta_2} \eta_r)^q, \quad (46)$$

where C_{2q} are constants. Equation (46) implies $\langle |\delta_{\vec{r}} \omega|^{2q} \rangle \sim \langle (\eta_r)^q \rangle r^{q\zeta_2}$ and hence $\langle (\eta_r)^q \rangle \sim r^{\gamma_q}$ with

$$\gamma_q = \zeta_{2q} - q\zeta_2. \quad (47)$$

An expression analogous to Eq. (47) has been proven for Kraichnan's model of passive scalar advection [37,38]. We note that Eq. (46) follows if

$$\eta_r \sim \frac{(\delta_{\vec{r}} \omega)^2}{r^{\zeta_2}} \quad (48)$$

which is the two-dimensional counterpart of Eq. (33). It is straightforward to show that the hypothesis Eq. (46) implies Eq. (40). Denoting η_r in box $\mathcal{R}_r(i)$ by $\eta_r^{(i)}$, we have

$$p_i(r) = \frac{r^2 \eta_r^{(i)}}{L^2 \langle \eta \rangle}. \quad (49)$$

Since $\sum_i [\eta_r^{(i)}]^q \sim r^{-2} \langle (\eta_r)^q \rangle$, we get $I(q, r) \sim r^{2q-2+\gamma_q}$, from which Eq. (40) immediately follows.

Finally, we remark that if the measure p_i is defined with a parameter n as follows [27]:

$$p_i(\epsilon, n) = \frac{\int_{\mathcal{R}_i(\epsilon)} |\vec{\nabla} \omega|^n d\vec{x}}{\int_{\mathcal{R}} |\vec{\nabla} \omega|^n d\vec{x}}, \quad (50)$$

then the corresponding formula for the D_q based on this measure is

$$D_q = 2 + \frac{\zeta_{nq} - q\zeta_n}{q-1}. \quad (51)$$

VI. CONCLUSION

We have studied the enstrophy cascade regime of two-dimensional turbulence with linear drag. A previous theory for the power law exponent of the energy wave-number spectrum is verified by direct numerical computation using a 4096×4096 lattice. We also calculate the vorticity structure functions numerically and show that they exhibit anomalous scaling in the presence of drag. The values of the structure function scaling exponents ζ_{2q} are measured and found to agree with the prediction by previous theory. We then compute the probability distribution function $\bar{P}_r(X_{\vec{r}})$ of the standardized vorticity difference $X_{\vec{r}}$ and find that $\bar{P}_r(X_{\vec{r}})$ develops exponential and stretched-exponential tails at small values of r . The theoretical expression for $\bar{P}_r(X_{\vec{r}})$ is shown to give predictions that agree well with the numerical results for a wide range of r . A measure based on the local viscous enstrophy dissipation rate η is studied in terms of its Rényi dimension spectrum D_q , and is found to be multifractal. The intermittency in η is connected to the intermittency in vorticity difference by a two-dimensional analog of the refined similarity hypothesis, and we derive a formula that relates D_q to ζ_{2q} [23].

ACKNOWLEDGMENTS

This work was supported by the Office of Naval Research and by the National Science Foundation (Grant No. PHYS 0098632).

[1] M. C. Kelley and E. Ott, *J. Geophys. Res.* **83**, 4369 (1978).
 [2] G. D. Nastrom and K. S. Gage, *J. Atmos. Sci.* **42**, 950 (1985).
 [3] H. Kellay, X. L. Wu, and W. I. Goldburg, *Phys. Rev. Lett.* **80**, 277 (1998).
 [4] M. A. Rutgers, *Phys. Rev. Lett.* **81**, 2244 (1998).
 [5] J. Paret, M.-C. Jullien, and P. Tabeling, *Phys. Rev. Lett.* **83**, 3418 (1999).
 [6] C. N. Baroud, B. B. Plapp, Z.-S. She, and H. L. Swinney, *Phys. Rev. Lett.* **88**, 114501 (2002).
 [7] H. Kellay and W. I. Goldburg, *Rep. Prog. Phys.* **65**, 845 (2002).
 [8] G. Boffetta, A. Cenedese, S. Espa, and S. Musacchio, *nlin.CD/0505034*.
 [9] R. H. Kraichnan, *Phys. Fluids* **10**, 1417 (1967).
 [10] R. H. Kraichnan, *J. Fluid Mech.* **47**, 525 (1971).
 [11] K. Nam, T. M. Antonsen, Jr., P. N. Guzdar, and E. Ott, *Physica*

- A **288**, 265 (2000).
- [12] K. Nam, E. Ott, T. M. Antonsen, Jr., and P. N. Guzdar, Phys. Rev. Lett. **84**, 5134 (2000).
- [13] D. Bernard, Europhys. Lett. **50**, 333 (2000).
- [14] M. Chertkov, Phys. Fluids **10**, 3017 (1998).
- [15] K. Nam, T. M. Antonsen, Jr., P. N. Guzdar, and E. Ott, Phys. Rev. Lett. **83**, 3426 (1999).
- [16] E. R. Abraham, Nature (London) **391**, 577 (1998).
- [17] The general approach of using a stochastic model velocity field has also been widely applied in the treatment of other types of passive scalar problems. For example, see the original papers of R. H. Kraichnan, Phys. Fluids **11**, 945 (1968); J. Fluid Mech. **6**, 737 (1974), and the review articles of G. Falkovich, K. Gawedzki, and M. Vergassola, Rev. Mod. Phys. **73**, 913 (2001); and of B. I. Shraiman and E. D. Siggia, Nature (London) **405**, 639 (2000).
- [18] G. Falkovich and V. Lebedev, Phys. Rev. E **49**, R1800 (1994).
- [19] G. L. Eyink, Physica A **91**, 97 (1996).
- [20] A. Rényi, *Probability Theory* (North-Holland, Amsterdam, 1970).
- [21] P. Grassberger, Phys. Lett. A **97**, 227 (1983).
- [22] H. G. E. Hentschel and I. Procaccia, Physica D **8**, 435 (1983).
- [23] A more extensive version of our paper can be found online at eprint cond-mat/0503424. Among other matters, the more extensive version contains a treatment of the $f(\alpha)$ singularity spectrum.
- [24] G.-C. Yuan, K. Nam, T. M. Antonsen, Jr., E. Ott, and P. N. Guzdar, Chaos **10**, 39 (2000).
- [25] E. Ott, *Chaos in Dynamical Systems*, 2nd ed. (Cambridge University Press, Cambridge, England, 2002).
- [26] E. Ott and T. M. Antonsen, Jr., Phys. Rev. A **39**, 3660 (1989).
- [27] F. Városi, T. M. Antonsen, Jr., and E. Ott, Phys. Fluids A **3**, 1017 (1991).
- [28] Z. Neufeld, C. López, E. Hernández-García, and T. Tél, Phys. Rev. E **61**, 3857 (2000).
- [29] G. Boffetta, A. Celani, S. Musacchio, and M. Vergassola, Phys. Rev. E **66**, 026304 (2002).
- [30] C. Reyl, T. M. Antonsen, Jr., and E. Ott, Physica D **111**, 202 (1998).
- [31] G. Stolovitzky and K. R. Sreenivasan, Rev. Mod. Phys. **66**, 229 (1994).
- [32] U. Frisch, *Turbulence* (Cambridge University Press, Cambridge, England, 1995).
- [33] A. B. Chhabra, C. Meneveau, R. V. Jensen, and K. R. Sreenivasan, Phys. Rev. A **40**, 5284 (1989).
- [34] C. Meneveau and K. R. Sreenivasan, J. Fluid Mech. **224**, 429 (1991).
- [35] A. N. Kolmogorov, Dokl. Akad. Nauk SSSR **30**, 301 (1941).
- [36] A. N. Kolmogorov, J. Fluid Mech. **13**, 82 (1962).
- [37] R. H. Kraichnan, V. Yakhot, and S. Chen, Phys. Rev. Lett. **75**, 240 (1995).
- [38] M. Chertkov and G. Falkovich, Phys. Rev. Lett. **76**, 2706 (1996).